Paper ID: 449

Toward a better understanding of the microdroplet debonding on elementary fiber

Adam Leveziel[1*], Xavier Gabrion[1], Florian Boutenel[1], Gilles Bourbon[1], Sébastien Thibaud[1].

[1]*FEMTO-ST Institute, Applied Mechanics Department, SUPMICROTECH-ENSMM, Marie Louis Pasteur University, CNRS(Institute, Department, University/Company, Address)*
**adam.leveziel@femto-st.fr*

Abstract

Gaining insight into the mechanisms governing separation at the fibre/matrix interface is critical for controlling composite performance, as this interface is responsible for load transfer between the reinforcement and the matrix. In this context, microdroplet debonding tests performed on elementary fibres enable targeted investigation of interfacial behaviour. However, such tests have been monitored using surface-based microscopic observations, which do not provide access to the internal processes occurring within the material. Consequently, this study introduces an in-situ microdroplet debonding methodology implemented within a laboratory-scale micro-computed tomography system, enabling three-dimensional visualisation of the microdroplet during the debonding. A dedicated experimental setup based on silicon blades with fixed openings was developed. Interrupted debonding tests performed on a single epoxy resin microdroplet deposited on an elementary fibre allowed the observation of crack propagation at the fibre/matrix interface prior the complete droplet debonding. This work highlights the potential of combining microdroplet debonding tests with laboratory-scale µCT to access internal interfacial mechanisms that remain inaccessible using conventional surface-based observations, thereby providing an interesting work to develop for advancing the understanding of fibre/matrix adhesion in composite materials.

Keywords: *Microdroplet; Debonding; X-ray computed tomography; Crack propagation;*

1 Introduction

Organic matrix composites offer exceptional specific stiffness and strength, properties largely governed by the fibre/matrix interface which controls stress transfer and damage initiation. While macroscopic characterisation is often influenced by manufacturing variables such as fibre orientation, distribution, and porosity. Micro-scale testing on elementary fibres isolates interfacial behaviour from these structural dependencies. Among such methods, the microdroplet debonding test stands out as a primary technique for quantifying interface properties [1].

This test involves depositing resin droplets onto a single fibre and subsequently debonding it using two blades positioned on either side of the fibre. Once the blades are positioned close to the fibre [2], a vertical displacement is applied to the fibre until debonding occurs. Widely used

for characterisation, this test offers the advantage of focusing specifically on fibre/matrix adhesion properties, which critically influence the material's macroscopic behaviour [1].

Although microdroplet debonding tests have been extensively studied in the literature, they are, at best, monitored in-situ via microscopic observations, which precludes a comprehensive understanding of the debonding process [3,4,5]. Indeed, previous studies have identified two distinct cracking mechanisms leading to debonding: (i) abrupt separation resulting in immediate failure, and (ii) progressive crack propagation along the interface during droplet loading [6]. However, after analysing a significant number of debonded specimens, Laurikainen et al. [3] concluded that more advanced experimental approaches are required to elucidate these two cracking regimes and fully characterise interfacial behaviour.

In the pursuit of a refined understanding of interfacial cracking, ex-situ fragmentation tests have demonstrated the feasibility of observing 3D strain and crack propagation in hemp fibres within an epoxy matrix using X-ray tomography [7]. Similarly, other researchers have conducted in-situ tests on glass fibre/epoxy systems using synchrotron radiation with a resolution of 150 nm to better comprehend the mechanisms governing fibre/matrix separation [8].

Consequently, the objective of the present study is to enhance the understanding of the phenomena governing microdroplet debonding. To this end, a protocol for interrupted in-situ microdroplet debonding tests has been developed.

2 Material and methods

2.1 Blades

To achieve minimal voxel sizes during in-situ laboratory-scale X-ray tomography, specimens must be positioned as close as possible to the X-ray source, necessitating a highly compact debonding setup. Furthermore, since both the blades and the droplet remain within the field of view throughout the acquisition, material selection is critical to mitigate imaging artefacts. Given the relatively low density of composite samples compared to metals [9], conventional metallic blades can induce severe density-related artefacts [10], potentially obscuring the fibre/matrix interface within the droplet.

Consequently, blades were fabricated from silicon. Preliminary trials, involving an epoxy droplet on flax fibre placed within a silicon structure, demonstrated that the interface remains visible despite minor artefacts. Beyond its compatibility with the samples of this study, silicon offers the advantage of precise machining via cleanroom processes. This enables the creation of complex geometries, including apertures of only a few tens of micrometres. The objective, therefore, was to develop blades compatible with the tensile machine jaws, featuring fixed apertures of 30 µm or 50 µm. Additionally, the blade tip thickness must be minimised to allow insertion between adjacent droplets. During deposition, fibre droplets may be positioned in close proximity. Excessively thick blades would prevent proper positioning between them.

The blades were manufactured using Deep Reactive Ion Etching (DRIE) on 4-inch wafers with a thickness of 380 µm. This method allowed for the production of varying blade apertures to accommodate different fibre types, also achieving a blade tip thickness of 30 µm.

The geometry of the blades and jaws is illustrated in Fig. 1a–b. Three contact points between the jaw and the blades are highlighted in yellow. They ensure isostatic positioning, allowing the blades to be correctly aligned within the machine's reference frame.

A Finite Element Analysis (FEA) was conducted to validate the blade geometry, as presented in Fig. 1c–d. Given the vertical axial symmetry of the design, only the upper half right side of the geometry was modelled, focusing on the region primarily subjected to stress during droplet loading. A point load of 1 N was applied to a blade tip. Based on the authors' experience, loads on the tested materials reach up to 0.35 N during droplet loading. Consequently, this scenario represents a worst-case condition (misaligned fibre causing single-blade loading during debonding) with a safety factor of approximately 3.

The simulation utilised 2D elements, with mesh refinement applied to areas likely to exhibit stress concentrations due to loading and geometric variations. The results indicated a maximum stress concentration of 558 MPa. Although the typical maximum allowable stress for silicon is often cited around 500 MPa, given the conservative nature of the worst-case scenario and the applied safety factor, the geometry is deemed valid for microdroplet debonding applications.

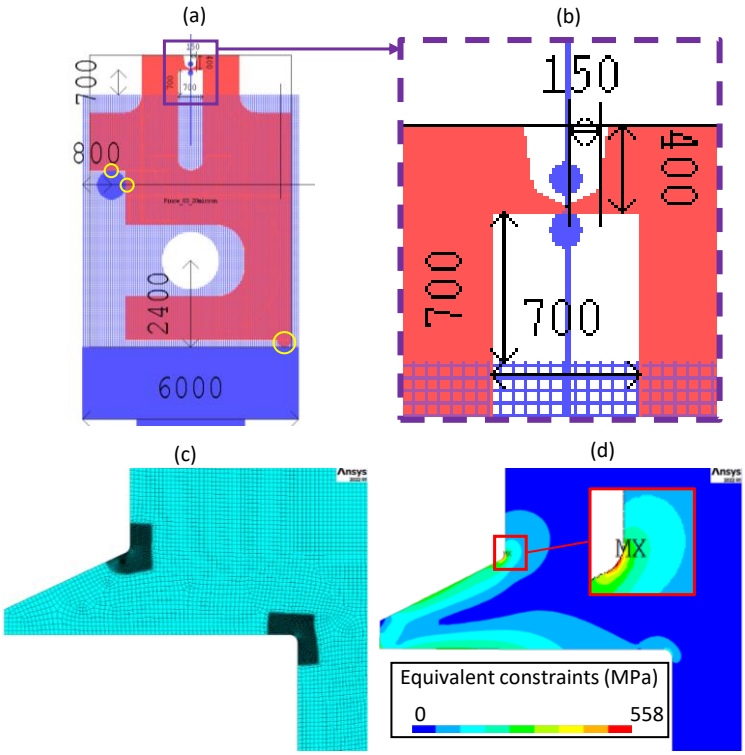

Figure 1. (a) Drawing of the blades in red, the jaw of the tensile machine in blue and a representation of the droplets with the fibres in between the two blades. (b) Zoom inside the two blades, (c) mesh of the geometry, (d) Equivalent constraint in one blade with a vertical loading of 1N.

2.2 Microdroplets preparations

Flax fibres derived from a unidirectional fabric (FlaxTape, EcoTechnilin, France) were functionalised by depositing iron oxides. These oxides were synthesised in situ in the presence of the fibres via the alkaline coprecipitation of iron (II) and iron (III) chlorides. The functionalised

fibres were supplied by the Biopolymers, Interactions, Assemblies Laboratory (INRAE, BIA, Nantes, France).

Prior to droplet deposition, the fibres were conditioned at room temperature and ambient humidity. To facilitate handling and testing, single fibres were carefully manually separated from the tape. Each isolated fibre was then mounted onto a paper frame, with both ends secured using cyanoacrylate adhesive.

Subsequently, microdroplets of Greenpoxy 56 (SICOMIN Composites, France), prepared with a resin-to-hardener mass ratio of 100:36, were manually deposited onto the free length of each fibre using a metallic needle pre-coated with the resin mixture. The microdroplets were cured in a climatic chamber (MEMMERT, Germany) for 24 h at 23 °C and 50 % relative humidity, followed by a further 24 h at 40 °C. Before debonding experiments, the samples were stored within the climatic chamber.

To identify droplets suitable for debonding within our setup, the relative position of each droplet, the embedded length, and the local fibre diameter were determined using a digital microscope (VHX-5000, Keyence, Japan).

2.3 Setting up of the droplets inside the blades

The tensile testing machine employed in this study is a custom-built in-house machine, developed in previous work to offer more compact dimensions than conventional in-situ tensile machines. The system comprises a lower jaw that translates within the machine reference frame, while the upper jaw remains fixed, supported by a PVC tube. This machine is place inside the x-ray tomography machine, between the source and the tomograph camera (Fig. 2a).

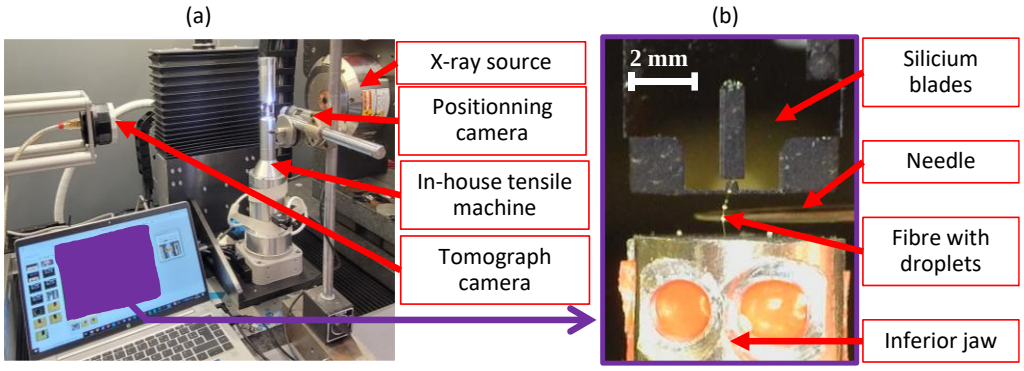

Figure 2. (a) Position of the tensile machine and camera. (b) View of the camera for the set-up of the fibre inside the blades.

To prepare the setup for debonding, the fibre initially embedded at both ends is cut in half to release one end from constraint. The previously described blades with fixed opening is then mounted onto the upper jaw. The paper frame is positioned against a thickness gauge on the

inferior jaw and secured by a screwed counter-jaw. The inclusion of the thickness gauge ensures that the fibre is centred within the blade aperture.

A digital microscope (Dino-Lite, AM4115ZT, Netherlands) is utilised to align the fibre within the blades. The lower jaw is gradually advanced towards the blade assembly. Through two access ports manufactured laterally and frontally in the PVC support, a fine needle is inserted to manoeuvre the fibre into the exact centre of the blades (Fig. 2b).

2.4 Observation and loading conditions

Interrupted *in-situ* tests [10], were conducted using radiography mode to assess the relative position of the blades and the droplet. These radiographic observations were performed using an X-ray micro-tomograph (EasyTom, RX Solutions, France). To maximise resolution, the smallest focal spot size was selected, operating at a source voltage of 60 kV and a current of 150 µA, coupled with a CCD camera (2018 × 1344 pixels²). In radiography mode, acquisition parameters included an exposure time of 1.4 s and an averaging of two frames.

Tomographic scans were acquired at various stages of the loading process. The same equipment and settings (focal spot, voltage, current, and acquisition parameters) were employed as for the radiography. The relative position of the source/tensile machine/CCD camera enabled a voxel size of 0.7 µm. Each tomographic scan required 32 minutes to complete. Reconstructions were generated from 512 projections using a filtered back-projection algorithm (XAct, RX Solutions, France), and the resulting volumes were visualised using VG Studio MAX 2025.

The reconstructions clearly exhibit the blades, droplet, and fibre, as well as brighter regions at the fibre/matrix interface corresponding to the iron oxides. Although the higher density of iron oxide (5 g/cm³) compared to the fibre and resin (1.5 g/cm³) results in greater x-ray attenuation (causing these areas to appear darker on raw radiographs), standard reconstruction conventions invert this contrast, rendering the oxides as brighter features in the final 3D volume.
The loading protocol was as follows: an initial tomography was performed prior to load application. The fibre was then advanced slowly towards the blades until contact was established. Subsequently, tomographic scans were acquired at intervals of every 10 µm of displacement, with a loading speed of 17 µm/s.

3 Results

Figure 3 illustrates a droplet undergoing debonding during the *in-situ* test. Figure 3a depicts the droplet prior to debonding, revealing iron oxide on the fibre surface, a feature also evident in the reconstructed slices (Figs. 3b–c) highlighted in circle in yellow. Figures 3b and 3c present cross-sectional slices through the droplet under load, taken at displacement loads of 20 µm and 30 µm, respectively. In both images, a darker grey line traverses the field of view. This artefact arises from the density differential between the silicon substrate and the sample. Furthermore, these reconstructions have been processed using a non-local means denoising filter to obtain a better contrast.

Figure 3b reveals that a crack initiated on the left side of the fibre. By measuring the corresponding opening in Fig. 3c, a crack propagation of 15 µm is measured. This opening is likely facilitated by the fibre orientation relative to the loading blades. Specifically, within the plane of the slices, an angle of 94° is observed between the loaded section of the fibre and the

artefact induced by the blades. Consequently, this slight deviation promotes Mode I opening at the interface, thereby enabling the crack propagation to be visualised in these slices.

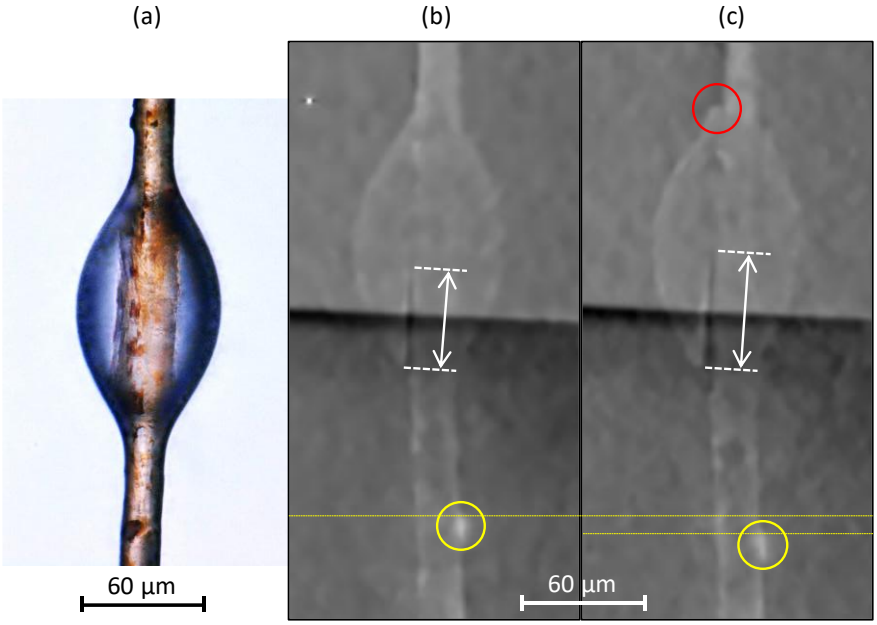

Figure 3. (a) Optical observation of the droplet prior debonding. Slices done coaxially of the axis of the loaded fibre section, parallel to the tip of the blades (b) at 20µm of loading and (c) at 30µm of loading.

Crack propagation occurred during the loading phase, as evidenced by several indicators of droplet debonding in the tomography acquired at 30 µm displacement. In Fig. 3c (circled in red), the meniscus at the top (the unloaded one) appears opened, presumably due to fibre slippage within the droplet. Furthermore, a displacement of 8 µm of an oxide agglomerate is measured between the two tomographic scans, as highlighted by the yellow lines positioned above the oxide agglomerate.

The displacement observed beneath the loaded droplet cannot be attributed solely to fibre deformation, as evidenced by the radiographs in Fig. 4. Captured immediately after the 30 µm load application and again five minutes later (perpendicular to the slices in Figs. 3b–c), these images reveal a downward movement of the satellite droplets consistent in magnitude with the displacement measured previously. This confirms a global fibre slip relative to the stationary central droplet, indicating that debonding occurred during the five-minute interval between acquisitions. Consequently, the interfacial crack initiated during the 20–30 µm loading step did not propagate immediately to the unloaded meniscus. Rather, its progression to complete debonding was time-dependent, occurring during the hold period between the two radiographic scans.

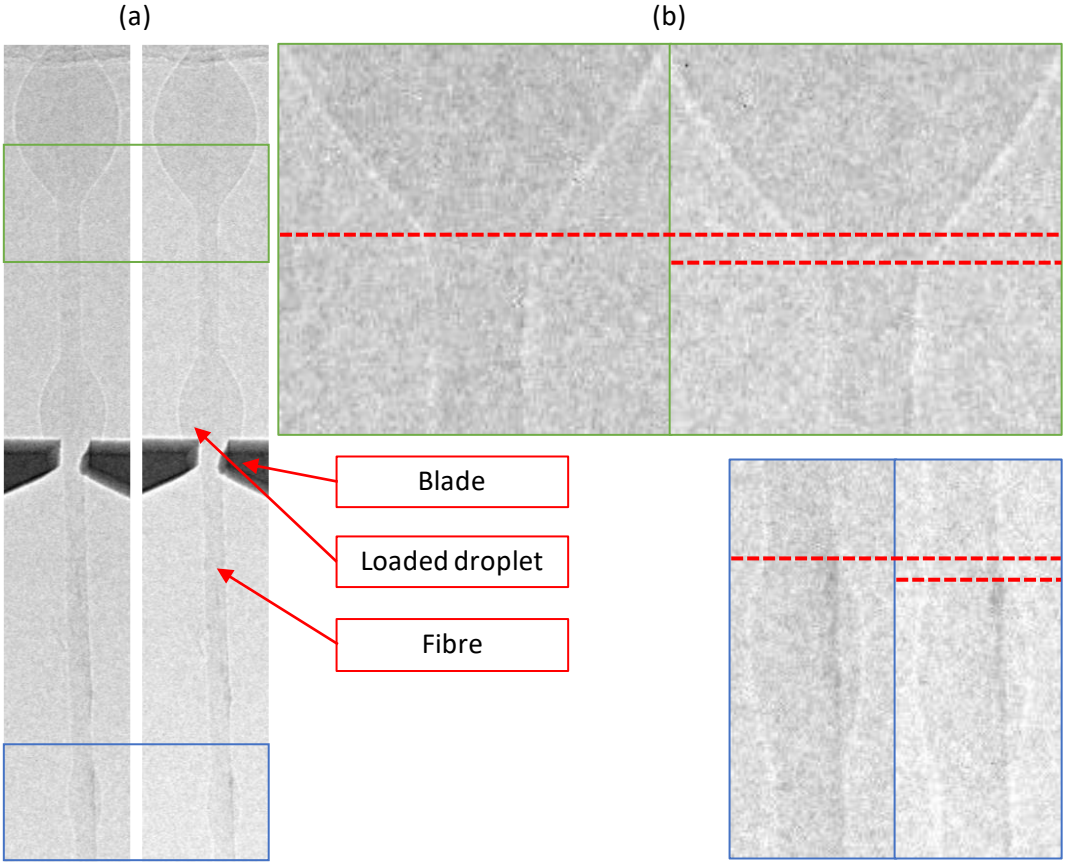

Figure 4. Radio images of the sample during the loading (a) after the 30µm load (left) and 5 minutes after (right). (b) Zoom images sattelite droplets above and under the debonded droplet.

4 Conclusions

The present study focuses on the implementation of in-situ microdroplet debonding tests within a laboratory-scale micro-computed tomography system to elucidate droplet debonding mechanisms.

To achieve this, silicon blades were fabricated. Their compatibility with the microdroplet test for 3D reconstruction was assessed. The blade geometry, featuring fixed openings, was validated via finite element analysis and manufactured using cleanroom processes.

Debonding test was conducted on a single epoxy resin microdroplet, demonstrating that crack observation is feasible in this configuration. The results enabled the visualisation of crack propagation prior the total debond of the droplet.

This study confirms the relevance of performing in-situ tests for microdroplet debonding to gain deeper insights into the underlying mechanisms. Future work should involve additional debonding tests to quantify crack propagation between loading increments prior to complete droplet failure.

Acknowledgements

This work received government funding administered by the French National Research Agency (ANR) as part of the 'France 2030' programme, under grant reference ANR-22-PERE-0005. This work was also supported by the EIPHI Graduate School (ANR-17-EURE-0002) and the Bourgogne-Franche-Comté Region, as well as partly supported by the RENATECH group and its technology platform at FEMTO-ST. The authors would like to thank the AMETISTE, MIFHySTO and MIMENTO platforms for the material and human resources provided, as well as Patrice Le Moal for the numerical simulations that enabled validation of the blade design, Vincent Placet for his assistance with interpreting the results and for his advice throughout the study, Valentin Sourbet for the design of the in-situ tensile testing machine and Baptiste Buet of the Biopolymers Interactions Assemblies Laboratory (INRAE, BIA, Nantes, France) for supplying the functionalised fibres.

References

1. Pantaloni D, Rudolph AL, Shah DU, Baley C, Bourmaud A. Interfacial and mechanical characterisation of biodegradable polymer-flax fibre composites. Compos Sci Technol. 2021;vol. 201, p. 108529.
2. Chou CT, Gaur U, Miller B. The effect of microvise gap width on microbond pull-out test results. Compos Sci Technol. 1994;vol. 51, p. 111–116.
3. Laurikainen P, Kakkonen M, Von Essen M, Tanhuanpää O, Kallio P, Sarlin E. Identification and compensation of error sources in the microbond test utilising a reliable high-throughput device. Compos Part A Appl Sci Manuf. 2020;vol. 137, p. 105988.
4. Thomason JL, Jenkins PG, Xypolias G. Microbond testing of the interface in glass fibre vinylester composites. Compos Interfaces. 2022;vol. 29, p. 695–709.
5. Pisanova E, Zhandarov S, Mäder E, Ahmad I, Young RJ. Three techniques of interfacial bond strength estimation from direct observation of crack initiation and propagation in polymer–fibre systems. Compos Part A Appl Sci Manuf. 2001;vol. 32, no. 3–4, p. 435–443.
6. Zhandarov S, Mäder E. Peak force as function of the embedded length in pull-out and microbond tests: effect of specimen geometry. J Adhes Sci Technol. 2005;vol. 19, p. 817–855.
7. Drouhet Q, Touchard F, Chocinski-Arnault L, Mellier D. 3D strain fields in a plant fibre composite during fragmentation test: Micro-CT based DIC and DVC. Compos Part B Eng. 2023;vol. 263, p. 110860.
8. Chatziathanasiou T, Lee Y, Villanova J, Stamati O, AhmadvashAghbash S, Fazlali B, Breite C, Sinclair I, Mavrogordato MN, Spearing SM, Mehdikhani M, Swolfs Y. Questioning the Representativeness of Damage Mechanisms in Single-Fiber Composites via In Situ Synchrotron X-Ray Holo-Tomography. Small. 2024;vol. 20, p. 2406168.
9. Le Gall M, Davies P, Martin N, Baley C. Recommended flax fibre density values for composite property predictions. Ind Crops Prod. 2018;vol. 114, p. 52–58.
10. Baissalov R, Sandison GA, Donnelly BJ, Saliken JC, McKinnon JG, Muldrew K, et al. Suppression of high-density artefacts in x-ray CT images using temporal digital subtraction with application to cryotherapy. Phys Med Biol. 2000;vol. 45, no. 5, p. N53–N59.
11. Garcea SC, Wang Y, Withers PJ. X-ray computed tomography of polymer composites. Compos Sci Technol. 2018;vol. 156, p. 305–319.